Applied Surface Science 538 (2021) 147652

Contents lists available at ScienceDirect

Applied Surface Science

journal homepage: www.elsevier.com/locate/apsusc

The role of amine in the sequestration of As (III) on functionalized indium tin oxide

Prescott E. Evans[a], Andrew J. Yost[b], Kayleigh A. McElveen[c], Qin-Yin Shi[d], Thilini K. Ekanayaka[a], Ashis K. Manna[e], Vicki Schlegel[d], Peter A. Dowben[a], Rebecca Y. Lai[c], Shikha Varma[e,*]

[a] Department of Physics and Astronomy, Theodore Jorgensen Hall, 855 North 16th Street, University of Nebraska-Lincoln, Lincoln, NE 68588-0299, USA
[b] Department of Physics, Oklahoma State University, Stillwater, OK 74078-3072, USA
[c] Department of Chemistry, Hamilton Hall, University of Nebraska-Lincoln, Lincoln, NE 68588-0304, USA
[d] Department of Food Science & Technology, 284 Food Innovation Center, University of Nebraska, Lincoln, NE 68583-0919, USA
[e] Institute of Physics, Sachivalaya Marg, Bhubaneswar, Orissa 751005, India

ARTICLE INFO

Keywords:
Arsenic
3-amino-propyl phosphonic-acid
XPS
Raman
IR
DFT

ABSTRACT

The influence of arsenite (As(III)) adsorption on 3-amino-propyl phosphonic-acid (3APPA) has been investigated using X-ray photoemission spectroscopy (XPS), vibrational IR and Raman spectroscopy. The functional amino group on 3APPA appears to play a significant role in the adsorption mechanism. Results of a combined experimental and theoretical investigation provide a comprehensive picture of the geometry and vibrational properties of 3APPA monolayers after interaction with arsenite. Experimental and scaled calculated IR properties display good agreement for the model case where NH_2 groups, located as pendant groups on 3APPA surface, interact with the adsorbed As-O network. A charge transfer to the As-O moiety is also indicated by XPS measurements and ionization potential maps generated by DFT. Thus, 3APPA, as a functionalized bio-adsorbant, shows promise towards detection and remediation of As(III) in contaminated wastewater.

1. Introduction

Arsenic pollution in drinking water poses severe health risks globally. Natural occurring sources as well as environmental pollution are responsible for arsenic contamination in ground water. The toxicity of arsenic contamination depends on the oxidation states, and the most toxic forms of Arsenic exist as Arsenites (i.e., arsenic trioxide, As(III)) and arsenates (arsenic pentoxide, As(V)) [1–3], with arsenite being nearly 60 times more toxic than the arsenate. These species are a serious health hazard as they are found in well drinking water [4,5] and may have affected populations as large as 100 million people globally. Safe detection of arsenite in drinking water is considered an important step for reducing this global public health problem. Easy detection of arsenite with cheap sensors can make a huge impact in alleviating this health hazard. In this regard, self-assembled monolayers (SAMs) for photoactive sensors and, because of the large surface area, offer opportunities for pollutant sequestration.

Self-assembled monolayers (SAMs) of functionalized alkanes (phosphonic acids, amines etc.) have been receiving immense attention in recent years due to their applications as corrosion-resistant coatings, biomolecular adhesive for sensors and as organic photovoltaics (OPV) [6].Tethering of dyes to SAMs of phosphonic acid (PA) also show potential for dye sensitized solar cells [7].

Phosphonic acid monolayers are also being considered as a means for engineering interfacial properties of many organic-semiconductor platforms. The synthesis and kinetics of monolayer formation have been discussed by a number of authors [8–20]. The fabrication of suitable monolayers usually involves tethering the phosphonic acid moiety at the surface with a spacer group providing some alignment of molecules and control of the orientation of the pendant tail group. This process has been applied for understanding many interfacial aspects related to work function change, surface energy tuning, redox activity etc. on several transparent metal oxide surfaces [8–13]. The molecular orientation of the spacer groups and the role of anchor groups is also important in controlling the functional properties [8,9].

Along with the formation of phosphonic acid monolayers, together with the alignment of molecules during the linkage of the phosphonic acid monolayer on a variety of substrates, most of the recent studies have investigated the modified interfaces as the templates for organic electronic devices, photovoltaic materials, solar cell etc. [8–20]. Phosphonic acid monolayers play an important role as a moiety for many applications, including interfacial electrode materials, in organic

* Corresponding author.
E-mail address: shikha@iopb.res.in (S. Varma).

https://doi.org/10.1016/j.apsusc.2020.147652
Received 19 May 2020; Received in revised form 3 August 2020; Accepted 22 August 2020
Available online 12 October 2020
0169-4332/ © 2020 Elsevier B.V. All rights reserved.

electronic devices. Tuning of the surface potential and work functions has been observed for the controlled growth and adsorption of aryl phosphonic acids on TiO_2 [9] as well as aromatic phosphonic acids on ZnO and ITO [10]. Several of these effects are influenced by the molecular dipoles in the adsorbate layer. For zinc phthalocyanine phosphonic acid layers, high rate constants for redox potential and organic photovoltaic (OPV) characteristics are guided by the orientation of the molecules on ITO [11]. High conversion efficiency for solar cell observed in phosphonic acid monolayer with carboxylic acid tail groups on ZnO nanorods is associated with the suppression of electron hole recombination [12]. Mesoporous SiO_2 material immobilized with phosphonic acid has shown potential for catalysis and drug delivery [13].

Deposition of organic-molecular SAMs on indium tin oxide (ITO) surfaces is also motivated by organic-inorganic templates for electronic devices and optical sensors [14,15]. 3APPA molecules adhere strongly to ITO leading to the formation of well-ordered semi-crystalline organic thin films. Annealing treatment enhances this linkage with several P—O bonds attaching to the metal oxide substrate [16,17]. While the phosphate anchor binds to the substrate, alkyl chains self-assemble parallel to each other with amine groups at the tail decorating the surface (Fig. 1). Such a mechanism forms an active layer at the surface where free amine groups are present as exposed pendant groups, facilitating the functionalization process. Some studies have explored alkane thiol, but they form disordered monolayers on the ITO surface [18].

Here we focus on the role these biomimetic platforms play in the adsorption of arsenite molecules. The interaction of arsenite with 3APPA monolayer has been investigated here by many experimental techniques and DFT based theoretical modelling. Such studies, though of significant importance, have not received much attention. Techniques like X-ray photoemission spectroscopy (XPS), Raman, IR vibrational analysis have been utilized here for a systematic understanding of the interactions. The presented investigation is a "proof-of-concept study", which comprehensively shows that exposed NH_2 tail groups on 3APPA monolayer display exceptional affinity for the arsenic species. The functional properties of the tail group assist in this conjugation which proceeds via a charge transfer to the As-O network from the amino group of 3APPA. Understanding such interaction mechanism, on this organic-inorganic system can provide superior platform for achieving remediation of arsenic species.

Based on density functional theory (DFT), we present here a description for the nature of interaction and adsorption of arsenite on 3APPA. Vibrational spectroscopic properties acquired from the first principle results have been assessed using experimental characterizations. The comparison validates the theoretical model proposed here with exposed surface-pendant NH_2 group playing crucial role in targeting the arsenite. Our theoretical approach illustrates quantum-mechanical level understanding and portrayal of the conjugation. Represented by ionization potential maps, charge transfer exchange has been explained through the surface complexation between amino tail and As (III). These observations are in agreement with the interpretation of XPS data on modified 3APPA monolayers. Results presented here show that the arsenite adsorption on 3APPA displays promise for the simple detection and treatment, i.e. removal of As (III) contamination in drinking water.

2. Experimental section

2.1. Materials and reagents

All reagents and solvents were used as received. Acetone (ACS, 99.5%) and trichloroethylene (ACS, 99.5%) were procured from Alfa Aesar (Haverhill, MA). Anhydrous ethyl alcohol (200 proof) was procured from Decon Technologies, Inc. (Santa Clara, CA). 3-Aminopropylphosphonic acid (3APPA, 98%) (Refer to Fig. 1 for a schematic diagram of the structures) and arsenic trioxide (As_2O_3, 99%) were procured from Sigma Aldrich (St. Louis, MO). Deionized water (DI H_2O) was purified using a Millipore Synergy system (18.2 MΩ•cm, Millipore, Billerica, MA) and was used to make all the solutions in this study. Indium tin oxide (ITO, 8–12 O) was purchased from Delta Technologies (Loveland, CO).

2.2. Sample preparation

The ITO substrate was cleaned by being placed in three different solutions, trichloroethylene, acetone, and ethanol, sequentially. The temperature of all three solutions was 50 °C, and the incubation time was 10 min per step. The cleaned ITO substrate was then placed in DI H_2O at room temperature for two hours prior to surface modification.

2.3. Modification of ITO surface with 3APPA and As_2O_3

The ITO substrate was immersed in a 1 mM ethanolic 3APPA solution for 17–19 h. The 3APPA-modified substrate was then placed in a 140 °C oven for 10 min to complete the annealing step. Next, the annealed substrate was exposed to 0.1 mM As_2O_3 (arsenite) for 17–20 h. All prepared samples were vacuum-sealed and stored in a dry and dark environment prior to the analysis.

2.4. Characterization of surfaces

In order to explore the properties of As(III) interaction with 3APPA monolayers, a systematic study utilizing XPS was executed at three different photoelectron emission angles. XPS was performed in an ultra-high vacuum (UHV) chamber which is equipped with an Al $K_\alpha$source (1486.6 eV) and a 150 mm SPECS PHOIBOS hemispherical analyzer. The base pressure of the system was better than $1x10^{-10}$ mbar at room temperature. All XPS spectra were collected at three different photoelectron emission angles: at 0° (normal takeoff angle), 40° and 80° (grazing incidence) with respect to the surface normal. The XPS spectrum acquired at 80° takeoff angle provides the information from the near-surface region of ca. 2 nm, instead of the 9 nm at 0°.

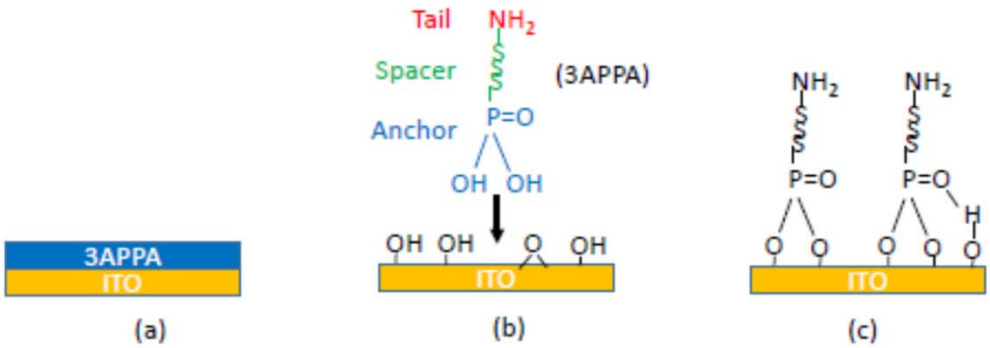

Fig. 1. A schematic of (a) the adlayer modification and (b) interaction of 3APPA with ITO, (c) bidentate/tridentate bonding of 3APPA on ITO.

The ATR- IR Spectroscopy studies have been undertaken on an Equinox 55 (Bruker Optics) spectrometer equipped with an air-cooled globar mid-IR source, a deuterated triglycine sulfate detector along with a MIRacle® single-reflection attenuated total reflectance (ATR) with a diamond/ZnSe crystal (Pike Technologies). Spectrum of the air was first acquired as instrument background. Samples were directly placed on the ATR crystal and were sufficiently pressed for achieving good contact. All spectra were recorded from 4000 to 510 cm^{-1} during 128 scans with a resolution of 4 cm^{-1}. The spectral data was processed on Opus NT version 6.5 (Bruker Optics). The data were first baseline corrected using rubber band method with 200 baseline points and then exported as data point table (.dpt) files for further analysis.

Raman scattering studies were performed in the backscattering geometry on a T64000 triple monochromator Horiba Jobin Yvon system equipped with a liquid nitrogen cooled CCD detector. Spectra were carefully acquired with a 514 nm laser. The power of the laser was below 1 mW and the resolution of the system was 0.5 cm^{-1}.

2.5. Computational details

The geometry optimization and vibrational frequncies have been calculated using quantum-chemical calculations. All density functional theory (DFT) calculations were carried out using the Wavefunction, Inc., Spartan'-18, suite of programs and the default convergence criteria were performed. The calculated vibrational frequencies were obtained with DFT using the typical B3LYP hybrid functional with the 6–31 + G* basis set for comparison with experiments. The B3LYP exchange–correlation functional was implemented for these calculations since it is accepted as standard in model chemistry framework for quantum mechanical calculations and provides vibrational spectroscopic properties for several molecular systems.

3. Results and Discussion:

XPS spectra of oxygen (O (1s)), phosphorus (P (2p)), indium (In (4 s)), nitrogen (N (1s)), and arsenic (As (3d)) were acquired for two types of samples: the 3APPA monolayers, and the 3APPA monolayers interacted with As (III). All the spectra have been calibrated using C (1s) core level binding energy of 284.6 eV. At all takeoff angles, O (1s) core level spectra (Fig. 2) contain four components: one at a binding energy of 529.3 ± 0.2 eV due to bulk O (with asymmetry caused by energy-loss processes), another at a binding energy of 530.6 ± 0.2 eV (from surface In—O—In and Sn—O) and a component at a binding energy of 531.9 ± 0.2 eV (from P—O—In, P═O… In, and surface In—OH). A low intensity O (1s) peak at 533.3 ± 0.2 eV is also observed, which shifts to 534.4 ± 0.2 eV, at an emission angle of 80°, indicating a somewhat reduced oxygen environment for the oxygen located away from the ITO interface, possibly as a result of hydrogen bonding or P—OH linking [19]. These results are in agreement with the XPS data obtained from phosphonic acid films on ITO [19,20]. Although several mechanisms have been proposed for the binding of phosphonic acid onto ITO surfaces, a reasonable conformation proposed by DFT studies is via O═P—O— bonding [19]. The success of the anchoring process for 3APPA on ITO is confirmed by XPS results seen here. This work also illustrates a dominance of bidentate/tridentate binding configuration through the O═P—O—In bonds.

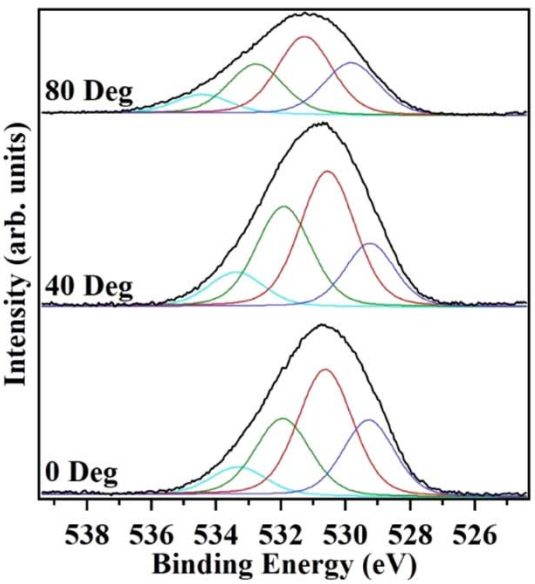

Fig. 2. The O (1s) core level XPS spectra, from 3APPA monolayers on ITO, taken at three photoelectron emission angles of 0°, 40°, and 80° with respect to surface normal.

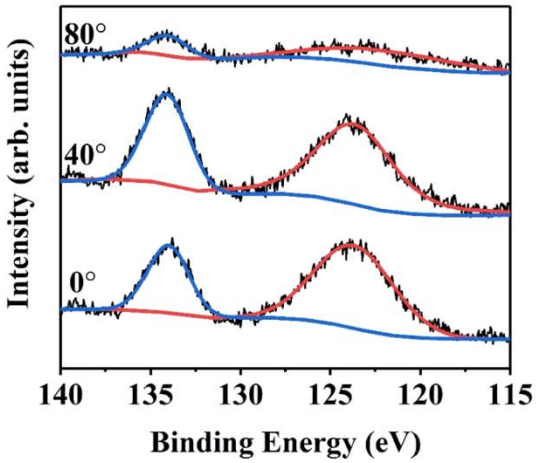

Fig. 3. The In (4s) and P (2p) core level XPS spectra from 3APPA monolayers on ITO, taken at three photoelectron emission angles of 0°, 40°, and 80° with respect to surface normal.

The P (2p) core level photoemission peak, observed at a binding energy of 134.0 ± 0.2 eV (Fig. 3), confirms the presence of phosphate groups and a bidentate type anchoring for 3APPA on ITO [21]. At a grazing photoelectron emission angle (80°), the intensity of this peak becomes weak as expected, since the P═O group is not much exposed. The In (4 s) signal from the ITO substrate also shows a similar reduction. These results strongly suggest a conformation where the 3APPA moiety is bonded to the oxide surface via P—O—In.

The N (1s) core level XPS signal (Fig. 4) confirms the presence of 3APPA with a photoemission feature at a binding energy of 402.4 ± 0.2 eV attributed to hydrogen bonded NH_2 [22] due to the protonation of amines (NH_3^+). The terminal amine groups on the tail of 3APPA, that are not hydrogen bonded and remain free, correspond to the feature at 400.92 eV [22] and the smaller peak at a binding energy of 399.3 ± 0.2 eV is assigned to a C-N bond [23]. An intensity ratio of 1:2 for protonated amine to terminal groups supports a successful 3APPA growth. For grazing photoelectron take-off angles, both nitrogen moiety concentrations being similar, a high propensity of protonated amine functional groups is available for coupling. Two higher binding energy features, at binding energies of 405.1 ± 0.2 eV and 406.8 ± 0.2 eV, are caused by the presence of some NO_2 on the surface.

Bio-adsorption properties of 3APPA were studied via arsenite interaction. After arsenite interaction, the XPS spectra of P (2p) and In (4s) appear (Fig. 5) nearly identical to those taken prior to the interaction. This ascertains that the overall SAM moiety or the linkage between 3APPA molecule and the ITO surface is not influenced much during the interaction. Also in agreement with Raman studies discussed below, there is no significant impact on the phosphate group either with

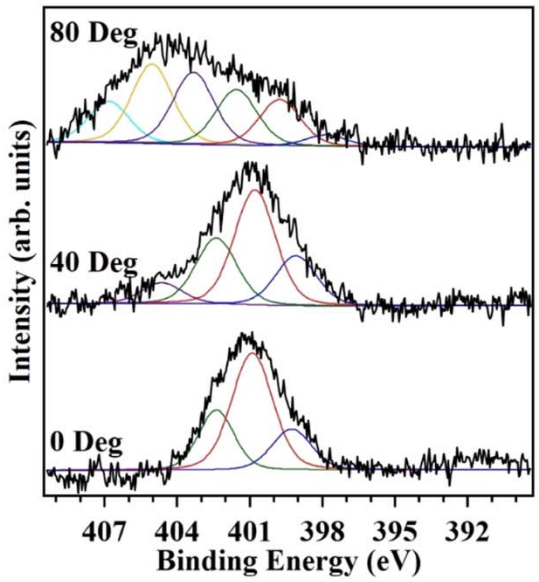

Fig. 4. The N (1s) core level XPS spectra from 3APPA monolayers on ITO, taken at three photoelectron emission angles of 0°, 40°, and 80° with respect to surface normal.

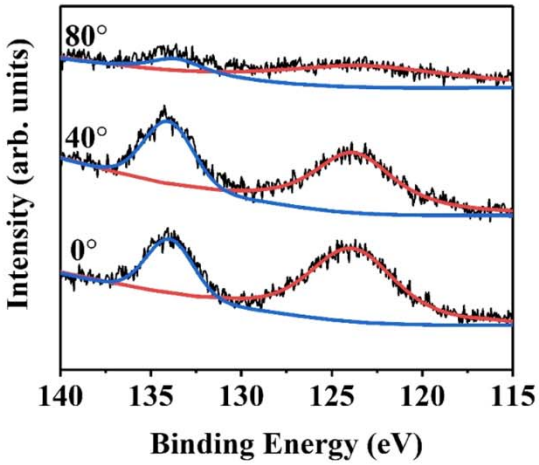

Fig. 5. The In (4s) and P (2p) core level XPS spectra XPS from arsenite interacted 3APPA monolayers on ITO, taken at three take-off angles 0°, 40°, and 80° with respect to surface normal.

arsenite interaction. Fig. 6 displays the O (1s) core level photoemission spectra after arsenite interaction. XPS is a surface sensitive technique and made more surface sensitive by increasing the take-off angle. As a result, angle dependent XPS studies provide crucial information for distinguishing interactions or charge transfer at bulk compared to that on the surface. Accordingly, XPS spectrum at the incidence angle of 0°, with respect to the surface normal, predominantly reflects the interactions occurring near the ITO interface compared to the spectrum at 80° which provides surface (within top ~2 nm) sensitive information. Discussing the spectra acquired at the incidence angle of 0°, O (1s) spectrum taken after arsenite interaction (Fig. 6) displays no discernable changes in the binding energy or area, compared to the XPS signal prior to interaction (Fig. 2). This strongly suggests that the interaction of arsenite does not induce any adsorption, modification or charge transfer to ITO. This is further confirmed by the results of Indium XPS which displayed no changes in In (4s) signal after arsenite interaction (Fig. 5), at any of the incidence angles, indicating that arsenite does not adsorb or interact with ITO substrate. Interaction with arsenite also does not influence the phosphate group, of the APPA, as displayed by P

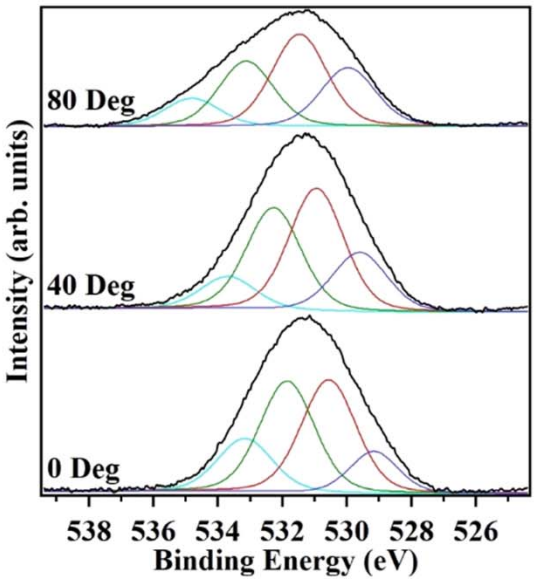

Fig. 6. The O (1s) core level XPS spectra from arsenite interacted 3APPA monolayers on ITO, taken at three photoelectron emission take-off angles of 0°, 40°, and 80° with respect to surface normal.

(2p) XPS results (Fig. 5). At higher emission angles (40° and 80°), the O (1s) core level XPS signal exhibits some shifts towards higher binding energies, after arsenite interaction, illustrating some charge transfer only near the surface, during arsenite linkage with 3APPA).

All three components in the main N (1 s) peak (Fig. 7), corresponding to the protonated amines (NH_3^+), terminal free amino groups (−NH−), and CN bonding, appear shifted towards lower binding energies of 400.7 ± 0.2, 399.4 ± 0.2, and 398.2 ± 0.2 eV, respectively. Bioadsorption of arsenite is also reflected by the enhanced ratio (1:1.2) of protonated amines relative to free amines. The weak NO_2 signal does not show much effect. Increased NH_2 and NH_3^+ content indicates that these functional groups may have participated in the adsorption process. Furthermore having electron donating centers, they may be efficiently transferring the charge during bio-conjugation. Functionalized graphite carbon nitride and chitosan based bio

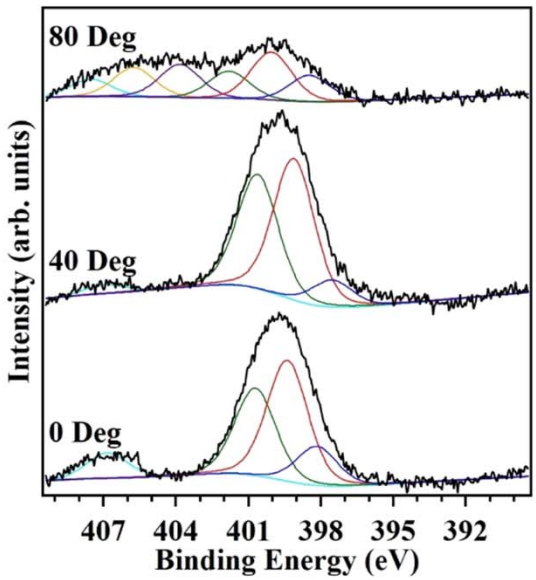

Fig. 7. N (1s) core level XPS spectra from arsenite interacted 3APPA monolayers on ITO, taken at three take-off angles 0°, 40°, and 80° with respect to surface normal.

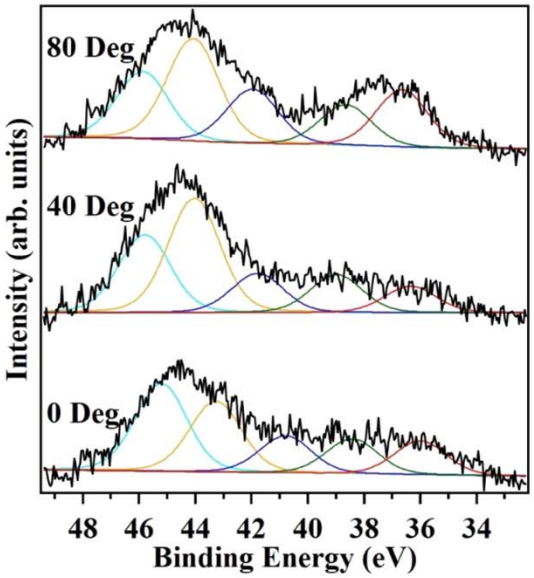

Fig. 8. The As (3d) core level XPS spectra from arsenite interacted 3APPA monolayers on ITO, taken at three photoelectron emission take-off angles of 0°, 40°, and 80° with respect to surface normal.

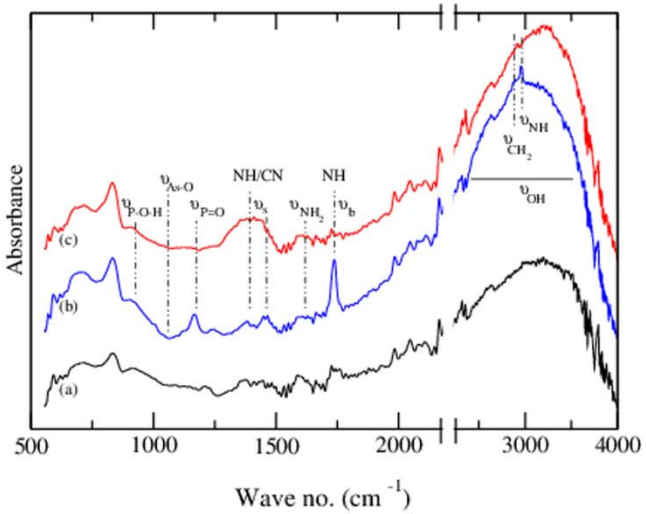

Fig. 9. The vibrational IR from (a) ITO, (b) 3APPA monolayers on ITO and (c) arsenite interacted 3APPA monolayers on ITO.

platforms also depict arsenite remediation by amino groups [24,25].

Such an adsorption coupled with electron transfer towards the arsenite layer is also confirmed by the As (3d) core level XPS spectra in Fig. 8. Here, in addition to an intense peak at 44.8 eV, due to As (III) [26], a secondary feature at 37.0 eV is seen in the As (3d) core level spectra (Fig. 8). This latter feature, which becomes strongest at large take off angles, with respect to the surface normal, is not expected for As^{3+} state and must reflect a reduced arsenic species, i.e. one with transfer of negative charge towards arsenite moiety [27] which ensures a bio-linking. Arsenite has a strong tendency to generate As—O type network and with charge transfer maximally occurring near the surface (at 80° angle in XPS), amino groups are once again demonstrated to be involved in the interaction. Earlier studies have shown that formation of As—O is an important route for the adsorption of organic arsenic [28,29]. All the XPS results presented here illustrate that the pendant NH_2 group on amine–rich 3APPA acts as the functional unit that promotes As (III) sorption. In addition, this binding is able to transfer electrons to the adsorbed As-O layer. This charge transfer is indicative of the ionic binding between the two moieties. These results are in agreement with the DFT model calculations discussed below.

Vibrational IR spectroscopy, in the region of 500–4000 cm^{-1}, has been used to understand the possible binding modes of 3APPA monolayers on ITO (Fig. 9). The presence of several fundamental modes, corresponding to NH and CN groups, testify to the successful formation of APPA monolayers (Fig. 9b).

The vibration bands corresponding to NH_2 stretch (υ_{NH2}) and N—H stretch (υ_{NH}) modes are respectively observed at 1619 and 2971 cm^{-1} [30,31]. Overlap of NH and CN stretching bands (υ_s) at 1392 and 1480 cm^{-1} as well as NH bending mode (υ_b) at 1740 cm^{-1} are also present [31,32]. The feature at 2899 cm^{-1} can be ascribed to the $-CH_2$ stretch (υ_{CH2}) mode [31–33] and is indicative of well-formed alkyl chains. The stretching vibrations υ_{OH} of the O—H group contributes to the characteristic broad vibrational feature at 3425 cm^{-1} (extending from 2000 to 4000 cm^{-1}).

The presence of fundamental P=O stretch mode $\upsilon_{P=O}$ at 1176 and P—O—H deformation $\upsilon_{P\text{-}O\text{-}H}$ at 926 cm^{-1} also suggest well formed 3APPA monolayers (Fig. 9b) [31,32]. In the vicinity of these modes, several profile variations relative to Fig. 9a, also confirm this. The existence of $\upsilon_{P=O}$ and $\upsilon_{P\text{-}O\text{-}H}$ suggest a bidentate/tridentate type bonding of 3APPA monolayers on ITO [33]. DFT studies have also been used by Paramonov *et al.* to identify the binding modes of octylphosphonic acid (OPA) on ITO. Structural optimization suggests that bidentate and tridentate type bondings are the most frequently occurring adsorption modes [19].

Once the 3APPA monolayers interact with As (III), the vibrational modes display several modifications (Fig. 9c). As_2O_3 is considered to form close knit networks with corner sharing AsO_3 pyramidal structures [34]. Although the symmetric stretching vibrational ($\upsilon_{As\text{-}O}$) mode from crystalline As_2O_3 is usually at 1050 cm^{-1} [34], it is not expected here due to the small concentration. However, many alterations at this location happen. Also, a distinct change in the IR profile (Fig. 9c), near the $\nu_{As\text{-}O}$ mode signifies the presence of arsenite. Severe distortion in IR profile (Fig. 9c), relative to un-interacted APPA (Fig. 9b), is accompanied by the disappearance of $\upsilon_{P=O}$ mode. This mode seems to be obscured in the IR when the As—O network bridges the 3APPA molecules of SAM. On the other hand XPS, which is a very sensitive technique for detecting atomic concentrations and oxidation states, shows that P=O still exists. Fig. 9c further reveals that NH stretch (υ_{NHs}) mode (2971 cm^{-1}) and N-H bending (υ_b) mode (1740 cm^{-1}) get severely diminished and shifted to 2919 cm^{-1} and 1730 cm^{-1}, respectively. Survival of NH_2 (υ_{NH2}) stretch mode (1480–1520 cm^{-1}), accompanied with enhanced intensity, shows involvement of amino groups in the coupling of arsenite with 3APPA. These observations are consistent with the XPS results, illustrating that the amines play an important role in these chemical interactions.

Although the ATR-FTIR demonstrates the successful biofunctionalization and arsenite adsorption, the results were further authenticated with Raman data. Prior to and post arsenite interaction, the Raman spectra display many charcteristic features (Fig. 10) ascribed to phosphonic groups [35]. These bands correspond to the IR data reported here (Fig. 9). The bands at 885, 967 and 1220 cm^{-1} are related to P—O—H symmetric, asymmetric stretching and deformation modes, respectively. Among the PO—H bands, the in-plane-deformation mode, δPO—H, appears very weak and broad in Raman spectrum. The vibrations for P=O correspond to weak shoulder at 1178 cm^{-1} [35] and do not seem to be influenced by arsenite, as indicated by XPS. In IR, however, changes were observed. These may be caused by the fact that techniques probe differently; with XPS being a surface sensitive technique, Raman spectroscopy probing via inelastic scattering, whereas IR vibrations involve absorption. After 3APPA interaction with arsenite, the As—O Raman mode is expected at 500 cm^{-1} [36]. However, it overlaps (Fig. 10b) with the bending and torsional modes of PO_4 group [36] as well as In—O mode from ITO [37]. In the review of Raman spectrum, post interaction, distortions in the NH and CN related bands

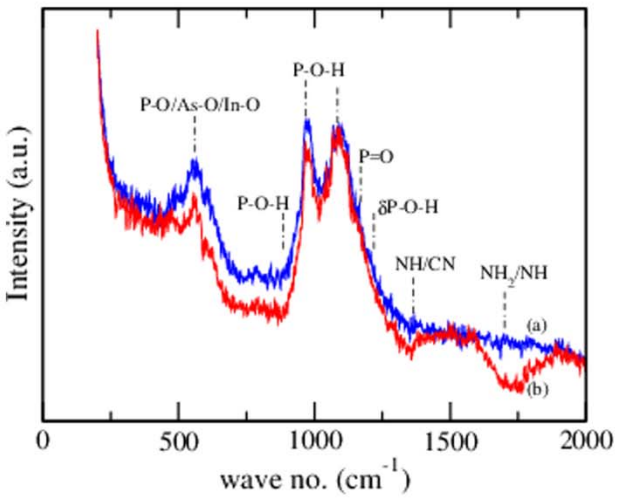

Fig. 10. The Raman spectra from (a) 3APPA monolayers on ITO and (b) arsenite interacted 3APPA monolayers on ITO.

become visible (Fig. 10b). The deformation region near 1354 cm^{-1} is enhanced by the overlap of NH and CN stretching whereas the broad band at 1630 cm^{-1} involves deformation in NH_2 and NH bending. These vibrational modes are in agreement to those delineated in IR and can be attributed to the arsenite sorption on 3APPA.

The DFT calculations were performed using B3LYP /6–31 + G* functional for 3APPA as well as post arsenite interaction. The calculated vibrational spectrum of 3APPA displays several well documented characteristic vibrations associated with the phosphonic groups, CN and NH. Though the calculated P—O—H mode appears at nearly similar wave number, some vibrational modes e.g. P═O, the overlapped NH/CN stretching and NH bending modes are red-shifted. This may be caused by the presence of extra molecular interactions, a common solid state effect, within well-formed 3APPA monolayers in experiments.

Still, one of the most intense IR bands on 3APPA, both theoretically (Fig. 11c) and experimentally (Fig. 11a), is the P═O mode supporting the presence of an 'intact' 3APPA on ITO. Other intense IR intensities in the calculated spectrum belong to the skeletal modes that fingerprint 3APPA, namely $\upsilon_{P\text{-}O\text{-}H}$ due to P—O—H vibrations, υ_s due to overlap of NH and CN, and υ_b due to NH bending.

Based on the XPS, ATR-IR and Raman results, some reasonable

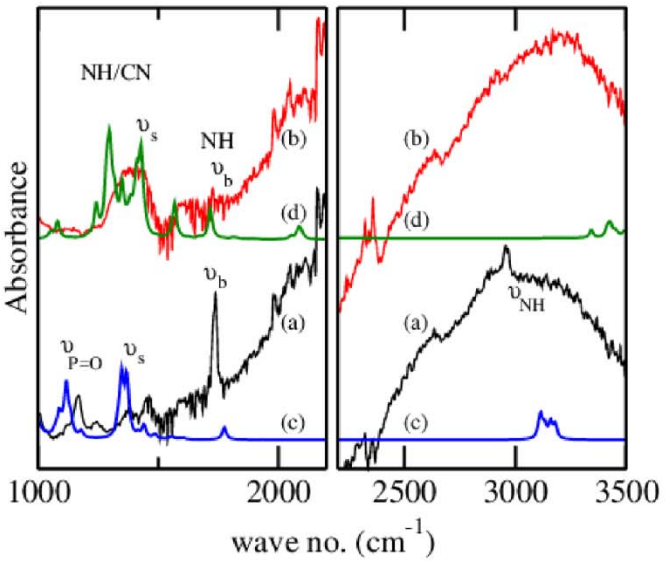

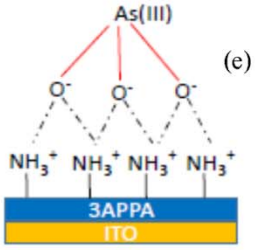

Fig. 11. The vibrational ATR-IR Experimental (a) 3APPA on ITO and (b) arsenite interacted 3APPA on ITO. Theoretical vibrational IR calculated with DFT/B3LYP method in a 6–31 + G* basis set (c) 3APPA and (d) arsenite interacted 3APPA on ITO. (e) Model for arsenite interacted 3APPA monolayers on ITO applied for calculation of DFT IR shown in (d).

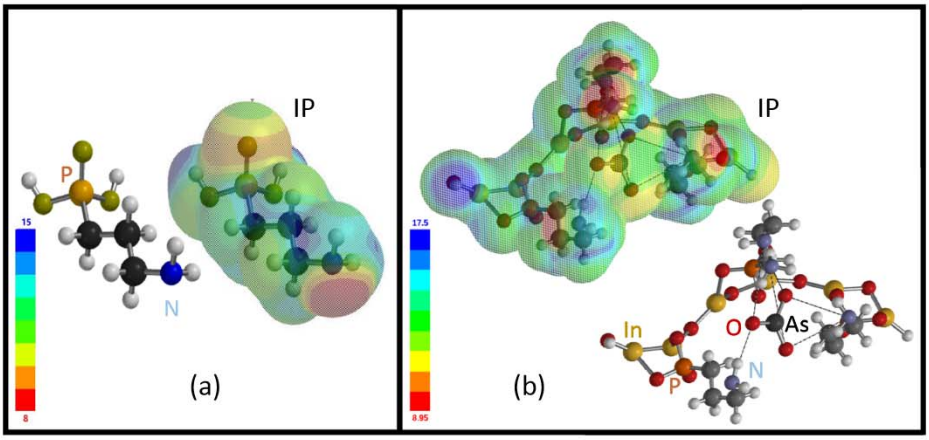

Fig. 12. The ionization potential (IP) maps calculated using the DFT/B3LYP functional, with a 6–31 + G* basis set, for (a) 3APPA and (b) arsenite interacted 3APPA on ITO.

conformations were hypothesized for As (III) conjugated 3APPA model. A possible interaction mechanism between As-O and amino group of 3APPA is illustrated in Fig. 11e. This was investigated via DFT and the results are presented in d.

As indicated above, the two close lying vibrational mode features (υ_s) in the DFT calculated spectrum (Fig. 11d) correspond to the overlapping vibrations of NH and CN. One of these modes is somewhat red shifted, compared to the measured spectrum, due to weaker coupling. The model geometry uses a small network, with not much long range interaction of As—O adsorbed on the tail-end amino groups. Still, although the calculated positions of the bands are not exactly the same, their trends and behaviors are similar to the measured data. The present approach can be utilized to extract ionization potential (IP) maps from DFT. The IP map designates an electron rich environment near N in amino group of 3APPA (Fig. 12a) which, in accordance with XPS, facilitates a charge transfer to the As-O network upon arsenite interaction (Fig. 12b).

4. Conclusions

The biomimetic platform of 3APPA monolayers has been utilized here to examine the role of amine functionalization towards bio-adsorption of arsenite. A structural model is depicted here, based on quantum level calculation, to elucidate the adsorption mechanism. It also was fully optimized at the B3LYP (DFT) level with the 6–31G* basis set and vibrational frequencies were calculated at the same level. A remarkable agreement between the experimental and the computed IR properties supports the configuration where adsorption is contributed through a charge transfer from pendant NH_2 group on 3APPA monolayers to the As-O network. Results show that 3APPA monolayers can act as functionalized bio-adsorbent for promoting conjugation with As (III) and hold promise for detecting and treating toxic arsenite in wastewater.

CRediT authorship contribution statement

Prescott E. Evans: Formal analysis, Investigation, Writing - review & editing. **Andrew J. Yost:** Conceptualization, Investigation, Supervision, Writing - review & editing. **Kayleigh A. McElveen:** Investigation. **Qin-Yin Shi:** Investigation. **Thilini K. Ekanayaka:** Investigation. **Ashis K. Manna:** Investigation. **Vicki Schlegel:** Investigation. **Peter A. Dowben:** Supervision, Conceptualization, Writing - review & editing. **Rebecca Y. Lai:** Conceptualization, Supervision, Writing - review & editing. **Shikha Varma:** Conceptualization, Investigation, Supervision, Writing - original draft.

Declaration of Competing Interest

The authors declare that they have no known competing financial interests or personal relationships that could have appeared to influence the work reported in this paper.

Acknowledgements

This project was supported in part by the Nebraska Public Power District through the Nebraska Center for Energy Sciences Research at the University of Nebraska-Lincoln under grant number 19-SE-2018 and the Nebraska Materials Research Science and Engineering Center (MRSEC) (grant No. DMR-1420645). Help of Santosh Choudhury with Raman spectroscopy is acknowledged.

Appendix A. Supplementary material

Supplementary data to this article can be found online at https://doi.org/10.1016/j.apsusc.2020.147652.

References

[1] A.P. Singh, R.K. Goel, T. Kaur, Mechanisms pertaining to arsenic toxicity, Toxicol. Int. 18 (2011) 87–93, https://doi.org/10.4103/0971-6580.84258.
[2] R.N. Ratnaike, Acute and chronic arsenic toxicity, Postgrad. Med. J. 79 (2003) 391–396, https://doi.org/10.1136/pmj.79.933.391.
[3] S. Chakraborty, F. Bardelli, M. Mullet, J.M. Greneche, S. Varma, J.J. Ehrhardt, D. Banerjee, L. Charlet, Spectroscopic studies of arsenic retention onto biotite, Chem. Geol. 281 (2011) 83–92, https://doi.org/10.1016/j.chemgeo.2010.11.030.
[4] T. Yoshida, H. Yamauchi, G. Fan Sun, Chronic health effects in people exposed to arsenic via the drinking water: Dose-response relationships in review, Toxicol. Appl. Pharmacol. 198 (2004) 243–252, https://doi.org/10.1016/j.taap.2003.10.022.
[5] N. Yogarajah, S.S.H. Tsai, Detection of trace arsenic in drinking water: Challenges and opportunities for microfluidics, Environ. Sci. Water Res. Technol. 1 (2015) 426–447, https://doi.org/10.1039/c5ew00099h.
[6] J.C. Love, L.A. Estroff, J.K. Kriebel, R.G. Nuzzo, G.M. Whitesides, Self-assembled monolayers of thiolates on metals as a form of nanotechnology, Chem. Rev. 105 (2005) 1103–1169, https://doi.org/10.1021/cr0300789.
[7] B.J. Brennan, M.J. Llansola Portolés, P.A. Liddell, T.A. Moore, A.L. Moore, D. Gust, Comparison of silatrane, phosphonic acid, and carboxylic acid functional groups for attachment of porphyrin sensitizers to TiO_2 in photoelectrochemical cells, Phys. Chem. Chem. Phys. 15 (2013) 16605–16614, https://doi.org/10.1039/c3cp52156g.
[8] M. Timpel, M.V. Nardi, S. Krause, G. Ligorio, C. Christodoulou, L. Pasquali, A. Giglia, J. Frisch, B. Wegner, P. Moras, et al., Surface Modification of ZnO (0001)−Zn with Phosphonate-Based Self-Assembled Monolayers: Binding Modes, Orientation, and Work Function, Chem. Mater. 26 (2014) 5042–5050, https://doi.org/10.1021/cm502171.
[9] J.B. Rivest, G. Li, I.D. Sharp, J.B. Neaton, D.J. Milliron, Phosphonic Acid Adsorbates Tune the Surface Potential of TiO2 in Gas and Liquid Environments, J. Phys. Chem. Lett. 5 (2014) 2450–2454, https://doi.org/10.1021/jz501050.
[10] U. Koldemir, J.L. Braid, A. Morgenstern, M. Eberhart, R.T. Collins, D.C. Olson, A. Sellinger, Molecular Design for Tuning Work Functions of Transparent Conducting Electrodes, J. Phys. Chem. Lett. 6 (2015) 2269–2276, https://doi.org/10.1021/acs.jpclett.5b00420.
[11] H.C. Lin, G.A. MacDonald, Y. Shi, N.W. Polaske, D.V. McGrath, S.R. Marder, N.R. Armstrong, E.L. Ratcliff, S.S. Saavedra, Influence of Molecular Orientation on Charge-Transfer Processes at Phthalocyanine/Metal Oxide Interfaces and Relationship to Organic Photovoltaic Performance, J. Phys. Chem. C 119 (2015) 10304–10313, https://doi.org/10.1021/acs.jpcc.5b02971.
[12] L. Yang, G. Chen, Y. Sun, D. Han, S. Yang, M. Gao, Z. Wang, P. Zou, H. Luan, X. Kong, J. Yang, Enhanced Photovoltaic Performance of QDSSCs via Modifying ZnO Photoanode with a 3- PPA Self-Assembled Monolayer, Appl. Surf. Sci. 328 (2015) 568–576, https://doi.org/10.1016/j.apsusc.2014.12.108.
[13] C. Weinberger, T. Heckel, P. Schnippering, M. Schmitz, A. Guo, W. Keil, H. C. Marsmann, C. Schmidt, M. Tiemann an René Wilhelm, Straightforward Immobilization of Phosphonic Acids and Phosphoric Acid Esters on Mesoporous Silica and Their Application in an Asymmetric Aldol Reaction, Nanomaterials 9 (2019) 249-260; doi:10.3390/nano9020249.
[14] H. Kim, C.M. Gilmore, A. Piqué, J.S. Horwitz, H. Mattoussi, H. Murata, Z.H. Kafafi, D.B. Chrisey, Electrical, optical, and structural properties of indium-tin-oxide thin films for organic light-emitting devices, J. Appl. Phys. 86 (1999) 6451–6461, https://doi.org/10.1063/1.371708.
[15] M.S. Wrighton, C.D. Frisbie, T.J. Gardner, D. Kang, Preparation and Characterization of Microelectrochemical Devices: Self-Assembly of Redox-Active Molecular Monolayers on Microelectrode Arrays, Microchemistry, Elsevier, 1994, pp. 495–506 10.1016/b978-0-444-81513-2.50041-7.
[16] T.J. Gardner, C.D. Frisbie, M.S. Wrighton, Systems for Orthogonal Self-Assembly of Electroactive Monolayers on Au and ITO: An Approach to Molecular Electronics, J. Am. Chem. Soc. 117 (1995) 6927–6933, https://doi.org/10.1021/ja00131a015.
[17] B. Vercelli, G. Zotti, G. Schiavon, S. Zecchin, A. Berlin, Adsorption of Hexylferrocene Phosphonic Acid on Indium-Tin Oxide Electrodes. Evidence of Strong Interchain Interactions in Ferrocene Self-Assembled Monolayers, Langmuir 19 (2003) 9351–9356, https://doi.org/10.1021/la030150y.
[18] S.H. Brewer, D.A. Brown, S. Franzen, Formation of thiolate and phosphonate adlayers on indium-tin oxide: Optical and electronic characterization, Langmuir 18 (2002) 6857–6865, https://doi.org/10.1021/la015720d.
[19] P.B. Paramonov, S.A. Paniagua, P.J. Hotchkiss, S.C. Jones, N.R. Armstrong, S.R. Marder, J.L. Bredas, Theoretical characterization of the indium tin oxide surface and of its binding sites for adsorption of phosphonic acid monolayers, Chem. Mater. 20 (2008) 5131–5133, https://doi.org/10.1021/cm8014622.
[20] S.A. Paniagua, A.J. Giordano, O.L. Smith, S. Barlow, H. Li, N.R. Armstrong, J.E. Pemberton, J.L. Brédas, D. Ginger, S.R. Marder, Phosphonic Acids for Interfacial Engineering of Transparent Conductive Oxides, Chem. Rev. 116 (2016) 7117–7158, https://doi.org/10.1021/acs.chemrev.6b00061.
[21] C. Tudisco, V. Oliveri, M. Cantarella, G. Vecchio, G.G. Condorelli, Cyclodextrin Anchoring on Magnetic Fe_3O_4 Nanoparticles Modified with Phosphonic Linkers, Eur. J. Inorg. Chem. 2012 (2012) 5323–5331, https://doi.org/10.1002/ejic.201200510.
[22] R.G. Acres, A.V. Ellis, J. Alvino, C.E. Lenahan, D.A. Khodakov, G.F. Metha, G.G. Andersson, Molecular structure of 3-aminopropyltriethoxysilane layers formed on silanol-terminated silicon surfaces, J. Phys. Chem. C. 116 (2012) 6289–6297, https://doi.org/10.1021/jp212056s.
[23] T.W. Scharf, R.D. Ott, D. Yang, J.A. Barnard, Structural and tribological characterization of protective amorphous diamond-like carbon and amorphous CN_x

overcoats for next generation hard disks, J. Appl. Phys. 85 (1999) 3142–3154, https://doi.org/10.1063/1.369654.
[24] C. Daikopoulos, Y. Georgiou, A.B. Bourlinos, M. Baikousi, M.A. Karakassides, R. Zboril, T.A. Steriotis, Y. Deligiannakis, Arsenite remediation by an amine-rich graphitic carbon nitride synthesized by a novel low-temperature method, Chem. Eng. J. 256 (2014) 347–355, https://doi.org/10.1016/j.cej.2014.06.045.
[25] L. Da Sacco, A. Masotti, Chitin and chitosan as multipurpose natural polymers for groundwater arsenic removal and As_2O_3 delivery in tumor therapy, Mar. Drugs. 8 (2010) 1518–1525, https://doi.org/10.3390/md8051518.
[26] S. Zhang, X. yan Li, J.P. Chen, An XPS study for mechanisms of arsenate adsorption onto a magnetite-doped activated carbon fiber, J. Colloid Interface Sci. 343 (2010) 232–238. https://doi.org/10.1016/j.jcis.2009.11.001.
[27] A. Mesarwi, A. Ignatiev, Interaction of Y overlayers with the GaAs(100) surface and oxidation of the Y/GaAs interface, Surf. Sci. 282 (1993) 371–379, https://doi.org/10.1016/0039-6028(93)90941-C.
[28] S.F. Lim, Y.M. Zheng, J.P. Chen, Organic arsenic adsorption onto a magnetic sorbent, Langmuir 25 (2009) 4973–4978, https://doi.org/10.1021/la802974x.
[29] C. Petit, G.W. Peterson, J. Mahle, T.J. Bandosz, The effect of oxidation on the surface chemistry of sulfur-containing carbons and their arsine adsorption capacity, Carbon N. Y. 48 (2010) 1779–1787, https://doi.org/10.1016/j.carbon.2010.01.024.
[30] J. Zhang, T. Ding, Z. Zhang, L. Xu, C. Zhang, Enhanced Adsorption of Trivalent Arsenic from Water by Functionalized Diatom Silica Shells, PLoS One 10 (2015) e0123395, https://doi.org/10.1371/journal.pone.0123395.
[31] M. Das, D. Mishra, T.K. Maiti, A. Basak, P. Pramanik, Bio-functionalization of magnetite nanoparticles using an aminophosphonic acid coupling agent: new, ultradispersed, iron-oxide folate nanoconjugates for cancer-specific targeting, Nanotechnology 19 (2008) 415101, https://doi.org/10.1088/0957-4484/19/41/415101.
[32] A.L.M. Ubaldini, M.L. Baesso, E. Sehn, F. Sato, A.R. Benetti, R.C. Pascotto, Fourier transform infrared photoacoustic spectroscopy study of physicochemical interaction between human dentin and etch-&-rinse adhesives in a simulated moist bond technique, J. Biomed. Opt. 17 (2012) 065002, , https://doi.org/10.1117/1.jbo.17.6.065002.
[33] A. Vega, P. Thissen, Y.J. Chabal, Environment-controlled tethering by aggregation and growth of phosphonic acid monolayers on silicon oxide, Langmuir 28 (2012) 8046–8051, https://doi.org/10.1021/la300709n.
[34] G. Sahaya Baskaran, N. Krishna Mohan, V. Venkateswara Rao, D. Krishna Rao, N. Veeraiah, Influence of aluminium ions on physical properties of PbO-P 2O5-As2O3 glasses, EPJ, Appl. Phys. 34 (2006) 97–106, https://doi.org/10.1051/epjap:2006049.
[35] W.W. Rudolph, Raman- and infrared-spectroscopic investigations of dilute aqueous phosphoric acid solutions, Dalt. Trans. 39 (2010) 9642–9653, https://doi.org/10.1039/c0dt00417k.
[36] G. Sahaya Baskaran, G. Little Flower, D. Krishna Rao, N. Veeraiah, Structural role of In2O3 in PbO–P2O5–As2O3 glass system by means of spectroscopic and dielectric studies, J. Alloys Compounds 431 (2007) 303–312, https://doi.org/10.1016/j.jallcom.2006.05.077.
[37] M. Marikkannan, M. Subramanian, J. Mayandi, M. Tanemura, V. Vishnukanthan, J.M. Pearce, Effect of ambient combinations of argon, oxygen, and hydrogen on the properties of DC magnetron sputtered indium tin oxide films, AIP Adv. 5 (2015) 017128, https://doi.org/10.1063/1.4906566.